

Abstract

The Arctic sea ice cover has changed drastically over the last decades. Associated with these changes is a shift in dynamical regime seen by an increase of extreme fracturing events and an acceleration of sea ice drift. The highly non-linear dynamical response of sea ice to external forcing makes modelling these changes, and the future evolution of Arctic sea ice a challenge for current models. It is, however, increasingly important that this challenge be better met, both because of the important role of sea ice in the climate system and because of the steady increase of industrial operations in the Arctic. In this paper we present a new dynamical/thermodynamical sea ice model, called neXtSIM in order to address this. neXtSIM is a continuous and fully Lagrangian model, and the equations are discretised with the finite-element method. In this model, sea ice physics are driven by a synergic combination of two core components: a model for sea ice dynamics built on a new mechanical framework using an elasto-brittle rheology, and a model for sea ice thermodynamics providing damage healing for the mechanical framework. The results of a thorough evaluation of the model performance for the Arctic are presented for the period September 2007 to October 2008. They show that observed multi-scale statistical properties of sea ice drift and deformation are well captured as well as the seasonal cycles of ice volume, area, and extent. These results show that neXtSIM is a very promising tool for simulating the sea ice over a wide range of spatial and temporal scales.

1 Introduction

The vast expanses of the Arctic ocean are one of the world's least accessible and least observed regions. The Arctic's thick cover of sea ice makes it inaccessible to ships and the constant motion and fracturing of the ice makes it treacherous to cross on foot. Over the last decades, the Arctic sea ice cover has thinned significantly (Lindsay and Schweiger, 2015), becoming largely seasonal, and losing part of its mechanical

TCD

9, 5885–5941, 2015

neXtSIM: a new Lagrangian sea ice model

P. Rampal et al.

Title Page

Abstract

Introduction

Conclusions

References

Tables

Figures



Back

Close

Full Screen / Esc

Printer-friendly Version

Interactive Discussion



strength. This is likely to change the sea ice dynamical regime, i.e. drift and deformation (e.g. Rampal et al., 2009; Zhang et al., 2012) with large potential impacts on the heat and momentum exchanges between the polar oceans, sea ice, and atmosphere (see e.g. Polar Group (1980) for a review). All climate models used nowadays include a sea ice model to get the best representation possible of both the Arctic and Antarctic climate and their respective roles in the climate system, like e.g. with respect to the origin(s) of the amplified positive temperature trend observed in the Arctic over the last decades (Bekryaev et al., 2010; Vaughan et al., 2013).

Since the late 70's, satellites for earth observations provided an unprecedented amount of information on the state, drift, and deformation of the Arctic ice cover over a remarkably large range of spatial and temporal scales. In particular, sophisticated multi-scale statistical methods were applied to this flow of observations leading to a significant improvement in our understanding of sea ice dynamics in particular. As a consequence, re-evaluation and re-tuning of largely-used sea ice models is being conducted by the research community. At the same time important shortcomings have been revealed by evaluating current climate models performance against observations with regard to sea ice trends and seasonal cycles for various quantities like sea ice extent, thickness and drift (e.g. Rampal et al., 2011; Stroeve et al., 2014). These results raised the question of potential missing physics in current sea ice models and/or incorrect treatment of the numerous interactions that all depend on the ice cover's mechanical behaviour (controlled by the sea ice rheological model), and state. This motivated the development of the new sea ice model presented in this paper, for which we put a particular focus on local sea ice dynamics and large-scale pattern of the sea ice cover in the Arctic.

The origin of most sea ice models used in the geophysical community today can be tracked back to the pioneering work done in the 1970s on the dynamical and thermodynamical modelling of sea ice. The first truly successful thermodynamical model of sea ice was published by Maykut and Untersteiner (1971), where they model the heat flux through sea ice and the resulting ice growth and melt. Semtner (1976) proposed

neXtSIM: a new Lagrangian sea ice model

P. Rampal et al.

Title Page

Abstract

Introduction

Conclusions

References

Tables

Figures



Back

Close

Full Screen / Esc

Printer-friendly Version

Interactive Discussion



neXtSIM: a new Lagrangian sea ice model

P. Rampal et al.

Title Page

Abstract

Introduction

Conclusions

References

Tables

Figures



Back

Close

Full Screen / Esc

Printer-friendly Version

Interactive Discussion



a simpler and more efficient model with only three vertical layers, more suitable for inclusion in general circulation models. He also suggested a “zero” layer model, where no information about the ice internal temperature exists. The zero-layer model has become very popular due to its simplicity and it is appropriate for applications within a time scale shorter than the seasonal scale and for thin ice. More advanced thermodynamical models for use in coupled modelling studies have been developed since the Semtner-model. These include for example the models by Bitz and Lipscomb (1999), Winton (2000), Ukita and Martinson (2001), and Huwald et al. (2005). These give a more accurate representation of the long-term evolution of the ice, important in particular for global climate models.

Coon et al. (1974) introduced the first realistic dynamical sea ice model, based on observations from the Arctic Ice Dynamics Joint Experiment (AIDJEX). In their model, sea ice was described primarily as a plastic material that deforms irreversibly once a critical internal stress state is reached. When the stress is sub-critical, however, the ice is modelled as an elastic material that deforms under stress, but returns back to its original shape when the stress is removed. Hibler (1979) replaced the elastic response of the AIDJEX model by a viscous one, producing the viscous-plastic model (VP). This made his model easier to solve numerically and easier to couple to ocean general circulation models. Hunke and Dukowicz (1997) suggested adding an elastic term to the VP model of Hibler (1979), producing the elastic-viscous-plastic model (EVP). This modification was based purely on numerical considerations making the model easier to parallelise, but offers no additional physical insights.

Modern, state of the art sea ice models are continuous models and include a thermodynamical component (commonly Bitz and Lipscomb, 1999) and a dynamical component (commonly Hunke and Dukowicz, 1997). In addition to the model features already mentioned these models generally include sub-grid scale parameterisations for the ice-thickness distribution (e.g. Thorndike et al., 1975; Rothrock, 1975; Hibler III, 1980; Lipscomb et al., 2007) and albedo evolution (e.g. Holland et al., 2012), possibly including melt-pond parameterisations (e.g. Flocco and Feltham, 2007). Parameteris-

ing the ice-thickness distribution is particularly important for low-resolution models and for modelling new-ice formation within the thick pack ice, while the albedo schemes are important for capturing the seasonal cycle and the onset of melt. In parallel, there was very active research on developing different solvers for the standard VP/EVP rheology (e.g. Lemieux et al., 2010), different rheologies (e.g. Tremblay and Mysak, 1997; Hopkins, 2004; Schreyer et al., 2006; Wilchinsky and Feltham, 2006; Sulsky et al., 2007; Girard et al., 2011; Tsamados et al., 2013; Herman, 2015; Rabatel et al., 2015; Dansereau et al., 2015), and wind and/or ocean-drag parameterisations (e.g. Lu et al., 2011; Lüpkes et al., 2012; Tsamados et al., 2014). These recent developments still need to be further evaluated regarding their contribution to better reproduce the vast complexity of sea ice dynamics.

Sea ice dynamics is very complex and shares many characteristics with earth crust dynamics, such as dynamical triggering and clustering of deformation events or earth/ice quakes. Both sea ice and the earth's crust are geophysical solids that can be viewed from the mechanical point of view as two dimensional plates due to their very small geometrical aspect ratio ($\mathcal{O}(10^{-6})$). These plates then experience planar internal stresses under the action of winds and ocean currents in the case of sea ice and magmatic currents of the mantle in case of the Earth's crust. Similarly to earth crust dynamics, sea ice dynamics is controlled by processes interacting and evolving over a wide range of spatial and temporal scales. Mechanical processes like fracturing and faulting are important as they both drive large scale sea ice drift and deformation patterns (e.g. Weiss et al., 2009). These processes are the expression of the mechanical damage of the ice pack which, as a result, looks more like an assembly of plates ($> \mathcal{O}(1 \text{ km})$) and floes ($< \mathcal{O}(100 \text{ m})$) than an intact solid plate. In addition to the quick damaging processes the slow formation of new ice is also important. Indeed, new ice formed in fractures and leads can act to fuse together broken ice and thus contribute to an effective mechanical strength recovery, or "healing". However, one should note that this recovery is much slower (i.e. several days or weeks) than the damaging process (i.e. several seconds or hours). The observed complex dynamical behaviour of the sea ice cover

neXtSIM: a new Lagrangian sea ice model

P. Rampal et al.

Title Page

Abstract

Introduction

Conclusions

References

Tables

Figures



Back

Close

Full Screen / Esc

Printer-friendly Version

Interactive Discussion



where m is the inertial mass, P is a pressure term, τ_a is the surface wind (air) stress, τ_w is the ocean (water) stress and τ_b is the basal stress in case of grounded ice. All these terms are defined in Sect. 2.2. The other symbols in Eq. (3) are: f , the Coriolis parameter; \mathbf{k} , the upward pointing unit vector; g , the gravity acceleration; η , the ocean surface elevation; and σ , the internal stress tensor.

The evolution of the internal stress is computed in two steps that correspond to:

$$\frac{D\sigma}{Dt} = \frac{\sigma^{(n+1)} - \sigma'}{\Delta t} + \frac{\sigma' - \sigma^{(n)}}{\Delta t}, \quad (4)$$

where superscripts n and $n+1$ correspond to the previous and current time steps, respectively. A first estimate of the internal stress, σ' , is computed without considering the damaging process:

$$\begin{bmatrix} \sigma'_{11} - \sigma_{11}^{(n)} \\ \sigma'_{22} - \sigma_{22}^{(n)} \\ \sigma'_{12} - \sigma_{12}^{(n)} \end{bmatrix} = \frac{E(A, d)}{(1 - \nu^2)} \begin{bmatrix} 1 & \nu & 0 \\ \nu & 1 & 0 \\ 0 & 0 & \frac{1-\nu}{2} \end{bmatrix} \begin{bmatrix} \dot{\epsilon}_{11} \\ \dot{\epsilon}_{22} \\ 2\dot{\epsilon}_{12} \end{bmatrix} \Delta t, \quad (5)$$

where E is the effective elastic stiffness depending on the concentration and the local damage (see Sect. 2.2), ν is Poisson's ratio and $\dot{\epsilon}$ is the strain rate tensor defined by $\dot{\epsilon} = \frac{1}{2} (\nabla \mathbf{u} + (\nabla \mathbf{u})^T)$. With this estimate of the internal stress, the failure criteria are checked. For the elements where the estimated internal stress σ' falls outside the failure envelope (defined in Sect. 2.2), the damage factor Ψ is set to the value for which the stress state

$$\sigma^{(n+1)} = \Psi \sigma', \quad (6)$$

is scaled back onto the failure envelope. For the elements for which the estimated internal stress σ' is inside the failure envelope, Ψ is simply set to 1. The corresponding damage source term Δd is defined as in Bouillon and Rampal (2015b) by the equation

$$\Delta d = (1 - \Psi)(1 - d^{(n)}). \quad (7)$$

neXtSIM: a new Lagrangian sea ice model

P. Rampal et al.

Title Page

Abstract

Introduction

Conclusions

References

Tables

Figures



Back

Close

Full Screen / Esc

Printer-friendly Version

Interactive Discussion



2.2 Dynamical component

In this subsection, we detail each term of the sea ice momentum equation (Eq. 3) and the underlying parameterisations.

The inertial mass m depends on the assumption made about the motion of the water present in leads: either the water in the leads moves as the ocean below or as the ice around it (Connolley et al., 2004). We choose the second hypothesis for our model, as we think it is more relevant for high resolution models and when the rheology allows for sharp transitions of sea ice concentration within the ice cover. Using this approach, the inertial mass m corresponds to the mass of ice and snow plus the mass of the water in the leads as $m = \rho_i h + \rho_s h_s + \rho_w h_w$, where ρ_w the reference density of seawater and h_w is the volume of water from the base of the ice to the sea surface per unit area. By isostasy, $\frac{\rho_w h_w}{(1-A)} = \frac{\rho_i h + \rho_s h_s}{A}$, and m is then given by

$$m = \frac{\rho_i h + \rho_s h_s}{A}. \quad (8)$$

The effective elastic stiffness $E(A, d)$ in Eq. (5) is defined as:

$$E(A, d) = Y e^{\alpha(1-A)} (1 - d), \quad (9)$$

where Y is the sea ice elastic modulus (Young's modulus) and α is the compactness parameter.

The failure envelope is defined in terms of the shear stress τ and the normal stress σ_N defined by:

$$\tau = \sqrt{\left(\frac{\sigma_{11} - \sigma_{22}}{2}\right)^2 + \sigma_{12}^2} \quad (10)$$

$$\sigma_N = \frac{\sigma_{11} + \sigma_{22}}{2} \quad (11)$$

respectively. The envelope is represented by a combination of a Mohr–Coulomb criterion, a tensile stress criterion and a compressive stress criterion, defined by:

$$\tau \leq -\mu\sigma_N + c \quad (\text{Mohr–Coulomb criterion}), \quad (12)$$

$$\sigma_N \leq \sigma_{N \max} \quad (\text{tensile stress criterion}), \quad (13)$$

$$\sigma_N \geq \sigma_{N \min} \quad (\text{compressive stress criterion}), \quad (14)$$

where μ is the friction coefficient, c is the cohesion and $\sigma_{N \max} > 0$ and $\sigma_{N \min} < 0$ are the maximal tensile stress and the maximal compressive stress, respectively. The friction coefficient μ for sea ice is chosen equal to 0.7, which is a common value for geo-materials (Amitrano et al., 1999) and seems to be scale-independent (Weiss and Schulson, 2009). The value of the cohesion c , $\sigma_{N \max}$ and $\sigma_{N \min}$ seem to be inversely proportional to the square root of the spatial scale (Weiss et al., 2007). Here we use this scaling relationship to define the value of c and $\sigma_{N \max}$ at 10 km from their estimate from in-situ measurements ($c_{\text{in situ}} = 40 \text{ kPa}$ and $\sigma_{N \max, \text{in situ}} = 50 \text{ kPa}$, Weiss et al., 2007). For $\sigma_{N \min}$, we apply the scaling relationship on the value estimated from lab experiments ($\sigma_{N \max, \text{lab}} = 15 \text{ MPa}$, Schulson, 2009).

The pressure P is set to avoid excessive convergence of highly damaged ice that would led to unrealistic local thickness of the ice cover. This term is parameterised as

$$P = P^* h^2 e^{\alpha(1-A)} \Phi \nabla \cdot \mathbf{u}, \quad (15)$$

where P^* is the pressure parameter and Φ determines if the pressure term is active or not. In our case, Φ is defined as a function of the divergence rate at the previous time step and is computed as:

$$\Phi = \begin{cases} 0 & \text{if } \nabla \cdot \mathbf{u}^{(n)} \geq 0 \\ \frac{1}{|\nabla \cdot \mathbf{u}^{(n)}| + \epsilon_{\min}} & \text{if } \nabla \cdot \mathbf{u}^{(n)} < 0, \end{cases} \quad (16)$$

where ϵ_{\min} is a parameter set to a small value to regularise the transition when the divergence rate is close to 0. The quadratic dependance on the mean thickness and the

neXtSIM: a new Lagrangian sea ice model

P. Rampal et al.

Title Page

Abstract

Introduction

Conclusions

References

Tables

Figures



Back

Close

Full Screen / Esc

Printer-friendly Version

Interactive Discussion



value of P^* used in this study ($P^* = 12 \text{ kPa}$) comes from Hibler (1986) and corresponds to the redistribution scheme of Thorndike et al. (1975) when it is applied to only one ice thickness category.

The air stress τ_a is computed following the quadratic expression:

$$5 \quad \tau_a = \rho_a c_a |\mathbf{u}_a - \mathbf{u}| [(\mathbf{u}_a - \mathbf{u}) \cos \theta_a + \mathbf{k} \times (\mathbf{u}_a - \mathbf{u}) \sin \theta_a], \quad (17)$$

where \mathbf{u}_a is the wind velocity, ρ_a the air density, θ_a the atmospheric turning angle, and c_a the atmospheric drag coefficient.

The oceanic stress τ_w is also computed following a quadratic expression, namely:

$$\tau_w = \rho_w c_w |\mathbf{u}_w - \mathbf{u}| [(\mathbf{u}_w - \mathbf{u}) \cos \theta_w + \mathbf{k} \times (\mathbf{u}_w - \mathbf{u}) \sin \theta_w], \quad (18)$$

10 where \mathbf{u}_w is the ocean velocity, ρ_w the reference density of seawater, θ_w the water turning angle, and c_w the water drag coefficient.

The basal stress τ_b is a term added to simulate grounded fast ice. It is parameterised as in Lemieux et al. (2015) by the expression:

$$15 \quad \tau_b = k_2 \frac{-\mathbf{u}}{|\mathbf{u}| + u_0} \max(0, h - h_c) e^{-C_b(1-A)}, \quad (19)$$

where k_2 is the maximum basal stress parameter, u_0 is the basal stress velocity parameter and C_b is the basal stress concentration parameter. The critical thickness from which the parameterisation starts acting is defined as $h_c = A \frac{H + \eta}{k_1}$, where k_1 is the critical thickness parameter and H is the ocean depth.

2.3 Thermodynamical component

20 In neXtSIM damaged sea ice recovers its mechanical strength through time via a healing process driven by the local temperature gradient between the bottom of the ice and the snow-ice interfaces. It is important to note that in the present model both the

thermodynamical healing and new ice formation (i.e. increase in ice concentration) act as negative feedbacks on sea ice deformation via the elastic stiffness parameterisation (see Eq. 9). The healing process is here assumed to decrease the effective compliance, defined as $C = \frac{1}{1-d}$, at a constant rate. The damage relaxation term S_d of Eq. (2) is then computed by

$$S_d = \frac{\left(1 - \frac{1}{C^{(n+1)}}\right) - d^{(n)}}{\Delta t}. \quad (20)$$

with $C^{(n+1)}$ given by

$$C^{(n+1)} = \max\left(\frac{1}{1 - d^{(n)}} - \frac{\Delta t}{T_C}, 1\right), \quad (21)$$

and where T_C is the compliance relaxation time. This relaxation time is here supposed to be inversely proportional to the temperature difference ΔT between the bottom and snow-ice interface, which is given by:

$$\Delta T = \frac{T_b - T_s}{\left(1 + \frac{k_i h_s}{k_s h}\right)}, \quad (22)$$

where T_b is the temperature at the ice base, T_s the temperature at the ice or snow surface, k_i is the heat conductivity of ice and k_s is the heat conductivity of snow. The compliance relaxation time is then defined as:

$$T_C = \max\left(\frac{T_d}{1000} \frac{40 \text{ K}}{\Delta T}, 0\right), \quad (23)$$

where T_d is the parameter controlling the healing rate. We use the constant 1000 and 40 K, which are typical values of effective compliance and temperature difference given

neXtSIM: a new Lagrangian sea ice model

P. Rampal et al.

Title Page

Abstract

Introduction

Conclusions

References

Tables

Figures

◀

▶

◀

▶

Back

Close

Full Screen / Esc

Printer-friendly Version

Interactive Discussion



by the model during winter, so that T_d can be interpreted as the time needed to heal the ice in winter conditions. The sensitivity to this parameter is discussed in Sect. 3. Also we limit T_C to be positive so that melting conditions alone ($T_s > T_b$) cannot damage the ice.

The other components of the thermodynamical model are similar to those in classical sea ice models. There are three thermodynamical source and sink terms corresponding to S_ϕ in Eq. (1), one for each of ice thickness, concentration, and snow thickness. The source/sink term for the ice thickness stems from the conservation of mass and can be written as

$$S_h = A\Delta h + (1 - A)\Delta h_{ow}, \quad (24)$$

where Δh is the change in level ice thickness and Δh_{ow} is ice formation in open water.

It is not possible to derive an equation for the concentration source/sink term S_A from first principles and the equation for it must be empirical. We use the form

$$S_A = (1 - A) \max(\Delta h_{ow}, 0)/h_0 + A \min(S_h, 0)/2h, \quad (25)$$

where h_0 is the demarcation thickness between thick and thin ice. Ice formation in the open water portion of the grid cell, h_{ow} , is calculated such that heat loss from the ocean that would cause super cooling is redirected to ice formation. This is an adaptation of the form suggested by Hibler (1979) in that he uses prescribed growth rates, but we calculate those depending on the atmosphere and ocean states, as described below.

The source/sink term for snow thickness, S_{h_s} , also stems from the conservation of mass and is

$$S_{h_s} = A\Delta h_s + h_s \min(0, S_A) + A \min(0, D - h/A)\rho_i/\rho_s. \quad (26)$$

The first term accounts for snow fall and melt, the second term removes snow due to the lateral melt of ice, and the third term converts snow into ice whenever the ice freeboard, D falls below the water surface due to snow loading. Energy needed to melt snow due to the lateral melt of ice is removed from the ocean as an additional heat flux.

neXtSIM: a new Lagrangian sea ice model

P. Rampal et al.

Title Page	
Abstract	Introduction
Conclusions	References
Tables	Figures
◀	▶
◀	▶
Back	Close
Full Screen / Esc	
Printer-friendly Version	
Interactive Discussion	



Thickness changes in level ice and snow are calculated using the zero-layer model of Semtner (1976). For this the incoming radiative fluxes are interpolated from the forcing data applying constant albedos to the incoming short-wave radiation of $\alpha_i = 0.64$ for the ice and $\alpha_s = 0.85$ for the snow (Maykut and Untersteiner, 1971). The turbulent heat fluxes are calculated using bulk formula for the sensible heat flux:

$$Q_{sh} = \rho_a c_p C_t |\mathbf{u}_a| (T_a - T_s) \quad (27)$$

and the latent heat flux:

$$Q_{lh} = \rho_a L_v C_q |\mathbf{u}_a| (q_a - q_s). \quad (28)$$

Here c_p is the atmospheric heat capacity and L_v is the latent heat of sublimation. The temperature difference, $T_a - T_s$ is taken between the ice surface and the atmosphere at 2 m, the same as the difference in specific humidity, $q_a - q_s$. We calculate the specific humidity using the formulation of Buck (1981). The drag coefficients C_t and C_q are set to 1.3×10^{-3} based on Ebert and Curry (1993). Fluxes between the ice and ocean, Q_{oi} , are calculated assuming the ocean underneath the ice must always be at the freezing point.

In order to produce realistic heat-fluxes through the ice, the thermodynamical ice model must be coupled to an ocean model. Here we use a simple slab ocean model that consists of a single ocean layer with one temperature and salinity point per grid cell. The flux of heat at the ocean surface is calculated as a weighted average of the ocean–ice and ocean–atmosphere fluxes:

$$Q_w = A Q_{oi} + (1 - A) Q_{oa}, \quad (29)$$

where Q_{oa} is the ocean–atmosphere flux. The ocean–atmosphere heat flux is calculated using the bulk formulas (Eqs. 27 and 28), with $C_t = 0.83 \times 10^{-3}$ and $C_q = 1.5 \times 10^{-3}$ (Gill, 1982) for the turbulent heat fluxes while the radiative heat fluxes are read in from the atmospheric forcing, applying a constant albedo of 0.07 to the short-wave flux.

neXtSIM: a new Lagrangian sea ice model

P. Rampal et al.

Title Page

Abstract

Introduction

Conclusions

References

Tables

Figures



Back

Close

Full Screen / Esc

Printer-friendly Version

Interactive Discussion



The change in ocean salinity is calculated assuming the total salt content of the ice–ocean system is conserved, resulting in a change in salinity of

$$\Delta S = \frac{(S_o - S_i)\rho_i\Delta h + S_o(\Delta h_s\rho_s - F_{fw}\Delta t)}{H_{ml}\rho_w - \Delta h\rho_i - (\Delta h_s\rho_s - F_{fw}\Delta t)} \quad (30)$$

for a change in ice and snow area mean thickness of Δh and Δh_s respectively, and where S_o and S_i are the ocean salinity and ice salinity, respectively, ρ_i and ρ_s are the ice and snow density, respectively, F_{fw} is freshwater flux at the surface, H_{ml} the mixed layer depth, and Δt the model time step.

When using a slab ocean, simulated ocean temperature and salinity have to be artificially maintained at realistic values because of the missing representation of both vertical and horizontal heat and salt exchanges within the ocean. Here, we use Newtonian nudging to relax the simulated ocean temperature and salinity towards the values of the uppermost ocean layer from a full ocean model (in this case the TOPAZ4 system, see Sect. 3.1). The local mixed layer depth from the full ocean model is also used as the mixed layer depth (H_{ml}) of the slab ocean model.

The slab-ocean model always resides on the same mesh as the ice model and the relative displacement of ice and ocean is ignored between remeshing steps. When the model mesh becomes too deformed and therefore needs to be remeshed, the temperature and salinity are interpolated from the old onto the new mesh using a linear interpolation and ignoring the displacement of the old mesh. This ensures that the temperature and salinity fields do not drift with the ice as the ice-model mesh moves.

2.4 Remeshing and remapping

Most sea ice models use an Eulerian approach for the advection. However, we believe that a purely Lagrangian approach as in Wang and Ikeda (2004) may be more suitable to preserve highly localised features (i.e. one cell wide ridged or open water areas) generated by the model. Purely Lagrangian schemes requires unstructured meshes and a procedure for mesh adaptation. Local mesh modifications can be done in parallel

and introduce very low numerical dissipation (Compère et al., 2009). It also allows local conservation (Compère et al., 2008).

In the purely Lagrangian approach, the vertices of the element (i.e. the nodes of the grid) move with the sea ice velocity \mathbf{u} . The material derivative is then simply equal to the temporal derivative $\left. \frac{\partial \phi}{\partial t} \right|_X$ relative to the moving mesh so that the quantities are naturally transported with the ice. The sea ice thickness and concentration, for example, are simply updated by:

$$h^{(n+1)} = h^{(n)} \frac{S^{(n)}}{S^{(n+1)}}, \quad (31)$$

and

$$A^{(n+1)} = \min \left(A^{(n)} \frac{S^{(n)}}{S^{(n+1)}}, 1 \right), \quad (32)$$

where $S^{(n)}$ and $S^{(n+1)}$ are the surface of the element at time steps n and $n + 1$. The variables defined at the nodes do not need to be updated.

In this approach the model mesh deforms as the ice cover itself deforms. When the mesh becomes too distorted the results of the finite element method are no longer reliable and the mesh must be adjusted, a process referred to as remeshing. In the current implementation the mesh is considered too deformed when the smallest angle of any triangle of the mesh is smaller than 10° . Using this criterion and the set up we use here, the mesh needs to be adapted on average every hour.

In order to save computational time the forcing fields are only interpolated onto the model grid after remeshing, or when new forcing fields are required. This means that even though the model grid drifts and deforms in-between remeshings the forcing seen by the nodes and elements of the model does not change. We checked that this method gives similar results than when we interpolate the forcing fields every time step. Indeed

as the remeshing criterion is global the error in the position of the forcing field is never larger than a single model element.

The new mesh is created by a version of the BAMG mesh generator by Hecht (1998) taken from the Ice Sheet System Model (Larour et al., 2012). This mesher can be instructed to preserve as many of the nodes from the old mesh as possible. The mesh is thus only modified in a limited number of locations, hereafter called “cavities”, at each remeshing. Doing this allows the model to track large expanses of drifting ice that is deforming very little without any artificial diffusion, since it is only necessary to interpolate values from the new grid to the old one inside the cavities. Outside the cavities the tracer values are not affected by the remeshing. For the variables defined at the nodes (i.e. the sea ice velocities, ...), a non-conservative linear interpolation is performed for the new nodes.

For the quantities that are defined at the center of the elements, a conservative remapping scheme is applied to each cavity independently. The cavities are defined as the smallest partitions of the mesh for which the external edges are the same before and after the remeshing. We implemented an algorithm that uses the information provided by BAMG (i.e. node-element connectivity and previous numbering of the preserved nodes) to efficiently detect the cavities and the intersections between the triangles of the old and new meshes. For each intersection, the corresponding integrated quantities are transferred from the old mesh to the new one. The process is fully conservative and generates only limited numerical diffusion.

3 Model evaluation and sensitivity

3.1 Simulation setup

For the model evaluation we force our model with the ocean state of the TOPAZ4 reanalysis (see Sakov et al., 2012), and with the atmospheric state of the Arctic System Reanalysis, Interim version (ASR-Interim hereafter) (<http://rda.ucar.edu/datasets/>)

neXtSIM: a new Lagrangian sea ice model

P. Rampal et al.

Title Page

Abstract

Introduction

Conclusions

References

Tables

Figures



Back

Close

Full Screen / Esc

Printer-friendly Version

Interactive Discussion



ds631.4/, Byrd Polar Research Centre/The Ohio State University (2012). Accessed 1 January 2014.) TOPAZ4 is a coupled ocean-sea ice system combined with a state-of-art Ensemble Kalman Filter data assimilation scheme of both ocean and sea ice variables, running at an average resolution of 12.5 km in the Arctic. The TOPAZ4 bathymetry is based on the 1 arcminute GEBCO bathymetry (Jakobsson et al., 2008) and the coastline is derived from the 5 m isobath. The main benefit of using the TOPAZ reanalysis in this context is its accuracy in simulating the location of the ice edge, and therefore to provide realistic forcing for ocean temperature and salinity. The ASR-Interim is a high resolution atmospheric reanalysis (30 km) known to reproduce particularly well the near-surface wind fields (Bromwich et al., 2015).

In order to simplify the forcing of the slab ocean with TOPAZ4, the domain of our model is defined from TOPAZ4 coastlines and open boundaries. The resulting mesh covers the Arctic and North-Atlantic Oceans, extending from an open boundary at 43° N in the North-Atlantic to an open boundary in the Bering Strait (see Fig. 1). Note that the ocean depth H used for the basal stress parameterization comes from the 1 arcminute ETOPO1 global topography (Amante and Eakins, 2009).

The oceanic forcing variables are sea surface height, velocity at 30 m depth, and sea surface temperature and salinity, which are provided as daily means by the TOPAZ4 system. We interpolate these quantities temporally and spatially onto the model mesh at run time using linear and bi-linear interpolation methods, respectively. The slab-ocean temperature and salinity are nudged towards TOPAZ4 and we found 30 days to be an appropriate nudging time scale for this set-up. This value allows our model to reproduce the location of the ice edge well without unduly affecting heat fluxes in the central Arctic. The heat flux resulting from the nudging is usually slightly below 0.5 W m^{-2} in the central Arctic in mid winter, which is a reasonable value (see e.g. Sirevaag et al., 2011).

The atmospheric forcing consists of the 10 m wind velocity, the 2 m temperature and mixing ratio, mean sea level pressure, total precipitation and the fraction of that which is snow, and the incoming short-wave and long-wave radiation. All of these quantities are

TCO

9, 5885–5941, 2015

neXtSIM: a new
Lagrangian sea ice
model

P. Rampal et al.

Title Page

Abstract

Introduction

Conclusions

References

Tables

Figures

⏪

⏩

◀

▶

Back

Close

Full Screen / Esc

Printer-friendly Version

Interactive Discussion



provided as three-hourly means by the ASR-Interim. Similarly to the oceanic variables, we interpolate them temporally and spatially onto the model grid at run time using a linear and bi-linear interpolation method, respectively. Both the atmospheric and oceanic forcing are progressively applied during a spin-up period of one day.

Our reference simulation starts on 15 September 2007 and ends on 9 October 2008. We choose this year because this is the only winter when the GlobICE (<http://www.globice.info>) and RGPS (Kwok et al., 1990) data sets overlap. The values of the model parameters that are used for this simulation are listed in Table 2. Damage is initially set to zero where sea ice is present. Initial sea ice concentration and thickness are interpolated from the sea ice of the TOPAZ4 reanalysis. The modelled ice thickness in TOPAZ4 is known to be unrealistically low on average compared to other Arctic ice–ocean coupled systems (Sakov et al., 2015) (<http://marine.copernicus.eu/documents/QUID/CMEMS-ARC-QUID-002-003.pdf>). We therefore scale it uniformly so that the initial total ice volume is the same as that from the PIOMAS reanalysis (Zhang and Rothrock, 2003, data downloaded from <ftp://pscfpt.apl.washington.edu/zhang/PIOMAS/> on 4 February 2014). Initial snow thickness is from the Warren et al. (1999) climatology, but we limit the snow thickness to 20 % of the ice thickness so that we don't get unrealistically thick snow on the relatively thin ice that was present at the start of the simulation.

3.2 Drag coefficient optimisation and evaluation of simulated ice drift

In neXtSIM, as in most classical sea ice models, the air and water drags depend on four parameters: c_a the air drag coefficient, θ_a the air turning angle, c_w the water drag coefficient and θ_w the water turning angle. The value of these four parameters have to be calibrated depending on which atmospheric and oceanic forcing are being used. The purpose of this section is to present how we proceed with this calibration for the present study.

neXtSIM: a new Lagrangian sea ice model

P. Rampal et al.

Title Page

Abstract

Introduction

Conclusions

References

Tables

Figures



Back

Close

Full Screen / Esc

Printer-friendly Version

Interactive Discussion



3.2.1 Basics of the method

By performing a scale analysis, it can be shown that the sea ice momentum equation (Eq. 3) is actually dominated by 3 terms: the ice internal stress, the surface wind drag and the surface ocean drag. This equation can therefore be written as:

$$\nabla \cdot (h\boldsymbol{\sigma}) + \boldsymbol{\tau}_a + \boldsymbol{\tau}_w = 0. \quad (33)$$

To prevent the rheology from affecting the optimisation process of the drag parameters, we only consider situations for which sea ice is in “free-drift”, i.e. situations where the internal stress term can be neglected in Eq. (33). By using Eqs. (17) and (18) and assuming that $|\mathbf{u}| \ll |\mathbf{u}_a|$, the solution of Eq. (33) then becomes:

$$\mathbf{u} = \mathbf{u}_w + Na \mathbf{u}_a, \quad (34)$$

where $Na = \sqrt{\rho_a c_a / \rho_w c_w}$ is the Nansen number. The first estimate of this number ($Na \approx 2\%$) was made by Fridtjof Nansen during the Fram expedition (1893–1896) by comparing the drift of his boat, while trapped in sea ice, to local wind and ocean velocities. The air and water density being considered as constant, the Nansen number only depends on the ratio between the two drag coefficients, c_a and c_w . In the free drift mode, calibrating the Nansen number is then equivalent to calibrating one of the drag parameters while keeping the other one constant.

The calibration method uses a full winter of sea ice drift data (here from the GlobICE dataset, <http://www.globice.info>), a reference run of one year starting in September 2007 and a series of short simulations restarted every 9 days from the reference run with the model being in free drift mode. To perform the simulation in free drift mode, we set the Young’s modulus Y and the pressure parameter P^* to 0. For each drift vector from the observation dataset, we compute the corresponding simulated drift vector from the 6 hourly Lagrangian sea ice displacement fields produced by the two sets of experiments, the reference run and the 9-day free drift run. The simulated drift from

Title Page

Abstract

Introduction

Conclusions

References

Tables

Figures

◀

▶

◀

▶

Back

Close

Full Screen / Esc

Printer-friendly Version

Interactive Discussion



the reference run is selected for the optimisation analysis only if it differs by less than 10% from the drift simulated by the free drift run. As in McPhee (1979), we also restrict the analysis to the range of ice speeds going from 7 to 19 km day⁻¹. As a result, about 15 000 vectors are selected from the 20 analysed periods of 9 days (from 31 October 2007 to 28 April 2008). As shown on Fig. 2, the identified free drift events are mainly located in the Transpolar Drift, in the Beaufort Gyre, and near the ice edge (i.e. in Greenland, Barents and Kara seas). Note that the number of identified free drift events also depends on the observation coverage, which is indeed high in the areas just mentioned.

3.2.2 Results of the method

By optimising the air drag parameters for these selected free drift vectors, we find an optimal value of $c_a = 0.0076$, corresponding to a Nansen number equal to $Na = 4.2\%$. Here, the optimal value is found to be higher than the classical values, which is consistent with the negative bias documented for ASR-Interim surface winds (Bromwich et al., 2015). Doing the same exercise for ERA-interim winds (Dee et al., 2011), which are frequently used to force large scale sea ice models, the optimal air drag coefficient is found to be $c_a = 0.0023$ (i.e. $Na = 2.3\%$), which is much closer to classical values. The scatter plots for each component of the selected vectors are shown in Fig. 3. For each component, the correlations between the simulated and observed free drift vectors are equal to 0.94 and 0.92, respectively, and the root mean square errors (RMSE) are equal to 2.5 and 2.3 km day⁻¹. The cumulative probability of the error in velocity is shown in Fig. 3, along with the median and mean error, which are equal to 2.3 and 2.8 km day⁻¹, respectively.

East Siberian and Chukchi Seas. These systematic errors may be partly explained by errors in the oceanic surface currents of TOPAZ, especially for the Beaufort Gyre. In the rest of the domain, the error on the mean winter drift is remarkably low, i.e. $< 1 \text{ km day}^{-1}$.

5 The mean drift speed, taken over the central Arctic, correlates closely with the mean wind speed taken over the same area. This is to be expected, since the wind is the main driver of ice drift. We do, however, expect to see a significant difference between the ice response to wind in summer and in winter, due mainly to changes in ice concentration and thickness. In order to assess this effect Fig. 8 shows the ratio of drift
10 speed over wind speed for the reference run, a model run forced with ERA-Interim, and the climatology of IABP buoy drift speed over ERA-Interim wind speed climatology. The two model runs considered here show a clear seasonal cycle in the drift-speed to wind-speed ratio. This is highest in summer, decreasing steadily from August to January, when it plateaus until April and then starts increasing again. Ólason and
15 Notz (2014) found that, over the 33 years they considered, the observed drift speed depends on concentration when concentration is low, thickness when concentration is high and is related to an increased number of active fractures in April–May. It is not clear how well our model captures this relationship since the results for only one year can be heavily influenced by the timing and intensity of storms passing through the
20 region. However, it is clear that the general shape of the observed time series for the drift-speed to wind-speed ratio is reproduced by the model, indicating that it captures correctly the transition between freely drifting ice and pack ice. In terms of magnitude, the drift-speed to wind-speed ratio for the run forced with ERA-Interim is slightly higher than the climatology. This is to be expected since both are based on ERA-Interim wind, the slight magnitude shift between the two being much likely the mark of the positive
25 trend in Arctic sea ice drift speed that was originally revealed from the analysis of the IABP dataset and reported by Rampal et al. (2009). Also, one can note a significant difference between the ratio time series of the reference run (in cyan) and that of the run forced with ERA-Interim (in blue). This can be explained by the fact that the winds

neXtSIM: a new Lagrangian sea ice model

P. Rampal et al.

[Title Page](#)[Abstract](#)[Introduction](#)[Conclusions](#)[References](#)[Tables](#)[Figures](#)[Back](#)[Close](#)[Full Screen / Esc](#)[Printer-friendly Version](#)[Interactive Discussion](#)

in ASR-Interim (used as forcing in the reference run) are weaker than in ERA-Interim, but this effect is counteracted in the model by tuning the drag coefficient, as discussed earlier.

3.3 Evaluation of simulated sea ice deformation and sensitivity to the healing time scale

One of the main differences of neXtSIM compared to other sea ice models is the rheology, which defines the link between internal stress and deformation. For the internal stress, only a few observations are available and cannot be directly used for a complete validation. However, as the two other dominant terms of the momentum equation (i.e. the ocean and atmospheric drag terms) seem well calibrated, the internal stress should also be correct. A good way to validate the new rheology is then to compare the simulated deformation fields to the large amount of data available from satellite products. The data used here are produced from the RGPS sea ice drift dataset with the method proposed by Bouillon and Rampal (2015a).

An interesting specificity of sea ice deformation is its strong localisation in space (see Fig. 9) and in time. This makes the use of a metric based on point-to-point comparison much too ambitious. Instead we compare simulated and observed deformation in a statistical sense using, among others, the powerful multiscale metrics introduced by Marsan et al. (2004) and Rampal et al. (2008). However, the strong spatial and temporal localisation can also be seen as a great advantage as it provides robust diagnostics that we will use for the validation itself.

The comparison with observation is focussed on the period January–April 2008, which has been identified as the period for which deformation is typically lower than during the rest of the year (see the annual cycle presented later in the paper). Figure 10 shows time series of the observed and simulated mean shear rate from January 2008 to April 2008. The deformation rates are computed at a spatial scale of 20 km and for 13 periods of 9 days. As in the previous sea ice drift evaluation, the model data are built to match the observations spatially and temporally. The correlation between the

neXtSIM: a new Lagrangian sea ice model

P. Rampal et al.

Title Page

Abstract

Introduction

Conclusions

References

Tables

Figures



Back

Close

Full Screen / Esc

Printer-friendly Version

Interactive Discussion



observed and simulated mean shear values is satisfactory, but we note that the model systematically underestimates the mean shear rate during this period.

Spatial scaling properties of sea ice deformation (or the degree of heterogeneity of sea ice deformation) can be studied from the analysis of Lagrangian trajectories, as e.g. in Marsan et al. (2004) who applied it to the trajectories of the RGPS dataset. Here we perform this analysis for both the model and the satellite observation, following the method used in Bouillon and Rampal (2015a), which is very similar to the one of Marsan et al. (2004), and which also gives an estimate of the error on the spatial scaling exponent. The spatial scaling analysis has been first applied to all the 13 snapshots corresponding to the 9-days periods between 1 January 2008 and 28 April 2008. However, in order to provide an accurate estimate of the spatial scaling, 4 snapshots have been discarded based on the large uncertainty we found associated with the power law fit on the observation data, and coming from the presence of noise on the estimated deformation. The values of the 1st order moment of the shear rate (here denoted \hat{e}_s) distribution obtained when gathering the selected snapshots is shown in Fig. 11 for different spatial scales. The power law $\langle \hat{e}_s \rangle \sim L^{-\beta}$ that fits the data (grey and black lines) corresponds to a scaling exponent β of -0.16 for the observations and -0.11 for the model. The departure from the power law fit at $L < 20$ km and $L > 500$ km comes from finite size effects (model resolutions and size of the Arctic basin, respectively). The scaling exponents $\beta(q)$ for the other moment orders of the shear distribution fit well with a quadratic function of q , whose curvature is equal to 0.13 for the observation and 0.07 for the model. This shows that, like observed deformations (Marsan et al., 2004; Rampal et al., 2008), the deformation simulated by the model is characterised by a multifractal spatial scaling.

Temporal scaling properties of sea ice deformation (or the degree of intermittency of sea ice deformation) can be studied from the dispersion of passive tracers (Rampal et al., 2008). Note that this approach is inspired by a classical methodology developed originally to study fluid turbulence (Richardson and Stommel, 1948; Batchelor, 1952). Here we perform the temporal scaling analysis for both the model and the observa-

neXtSIM: a new Lagrangian sea ice model

P. Rampal et al.

Title Page

Abstract

Introduction

Conclusions

References

Tables

Figures



Back

Close

Full Screen / Esc

Printer-friendly Version

Interactive Discussion



tions following the same method as in Rampal et al. (2008), using pairs of vertices of the model mesh and pairs of tracking points of the RGPS trajectory dataset, respectively. Indeed, in a Lagrangian modelling framework each vertices of the mesh can be considered as a passive tracer of sea ice, and directly compared with tracking points of the RGPS dataset. For each pair of vertices/RGPS points initially separated by a distance of ~ 30 km on average, a proxy of sea ice deformation is measured by looking at the relative variation of the distance between the two vertices/RGPS points for different time intervals. For the model the intervals are 0.25, 0.5, 1, 2, 4, 8, 16, 32 and 64 days, whereas the analysis for the RGPS trajectories only starts from a time interval of 2 days due to the limited temporal resolution of these data. The number of analysed measurements is similar to Rampal et al. (2008) and decreases from 630 000 for the 0.25 day interval to 2600 for the 64 days interval. Figure 12 shows the mean value of $|\dot{D}|$ for the different time scales for the model and the observations. A power law model $\langle |\dot{D}| \rangle \sim T^{-\alpha}$ from $T = 2$ to 64 days fits both the observed and simulated data very well, with the same scaling exponent $\alpha = 0.3$. Previous studies based on buoy data indicate that the scaling should also hold for smaller scales. This is not the case for the model data and cannot be verified from the RGPS data used in this study. The right panel of Fig. 12 indicates that the model only gives the right scaling exponent for healing time scales equal and larger than 7 days. We note that the order of magnitude of the healing time scale is consistent with the conclusion made in the previous section from the analysis of the sensitivity of the model performance with respect to sea ice drift.

The simulated mean value and spatial scaling exponent of the 3-days deformation evolves during the year of simulation (see Fig. 13), with much lower mean deformation between January and April, and a more negative scaling exponent in Summer than in Winter. We note that this behaviour, as well as the high variability from one 3 days period to the other, compares well with the results found by Stern and Lindsay (2009) from the analysis of the whole RGPS dataset.

neXtSIM: a new Lagrangian sea ice model

P. Rampal et al.

[Title Page](#)[Abstract](#)[Introduction](#)[Conclusions](#)[References](#)[Tables](#)[Figures](#)[Back](#)[Close](#)[Full Screen / Esc](#)[Printer-friendly Version](#)[Interactive Discussion](#)

tune the model to the applied forcing. The different albedo scenarios are “high albedo”, where we choose very high albedos of $\alpha_i = 0.7$ and $\alpha_s = 0.9$ and “temperature dependent albedo”, where the albedos depend on the surface temperature calculated in the model. This dependence is simply

$$\alpha = \begin{cases} \alpha' - \beta(T_s + 1) & \text{for } T_s > -1^\circ\text{C} \\ \alpha' & \text{otherwise,} \end{cases} \quad (35)$$

where α' is the freezing albedo (here set to 0.7 for ice and 0.9 for snow) and β is the temperature dependence of the albedo (here set to $\beta = 0.075$ for ice and $\beta = 0.124$ for snow, see Hunke et al., 2015). The two cases should constitute an upper and lower bound for the albedos. Indeed, in the “high albedo” case, substantially more ice remains at the end of the melt season compared to the reference run and in the “temperature dependent albedo” case the reduction in ice volume is substantially more rapid. It is likely that the best way forwards in tuning the system would be to use the temperature dependent albedos with reduced values for β .

Figure 14b and c show the modelled sea ice extent and area respectively, compared to satellite observations. The area is simply the total area covered by sea ice, while the extent is the total area of grid cells covered with more than 15 % of sea ice. The observations shown are the mean values and extremes for daily observations using the ASI algorithm AMSR-E (Kaleschke et al., 2001; Spreen et al., 2008, data obtained from the Integrated Climate Data Center, University of Hamburg, Germany, <http://icdc.zmaw.de>), OSI-SAF (EUMETSAT Ocean and Sea Ice Satellite Application Facility, 2015), NASA Team (Cavalieri et al., 1996), and Bootstrap (Comiso, 2000) products. Using these four products gives a good idea of the uncertainty involved in the satellite observations (N. Ivanova, personal communication, 2014 see also Ivanova et al., 2014).

In terms of extent, the results of the neXtSIM model are within the limits for the uncertainty estimates for the observations until the start of May. At this point the modelled melt is considerably more rapid than the observed one, leading to a difference of about 1.5 million km² at the beginning of June. From then, however, the observed melt be-

neXtSIM: a new Lagrangian sea ice model

P. Rampal et al.

Title Page

Abstract

Introduction

Conclusions

References

Tables

Figures



Back

Close

Full Screen / Esc

Printer-friendly Version

Interactive Discussion



comes much more rapid and the end result is that the modelled extent at the extent minimum is within the limits of the observations uncertainties. Changing the forcing or albedos does affect the melt substantially, but it does not alter the fact that the model fails to capture the two phased melt observed; a slow phase from early April to early June and a rapid phase from early June to early September.

In terms of total ice area, the model slightly overestimates the ice area during the freeze up, but is in good agreement with observations for the rest of the model run. This is, however, not the case when using the ERA-Interim forcing or the temperature dependant albedos since in those cases the melt is too rapid resulting in total ice area that is about 1.5 million km² smaller than in the reference run.

There is therefore a discrepancy between the modelled extent and area when compared to the observations, in that the modelled extent is too low during melt but the modelled area is correct. This seems to indicate that as the ice concentration is reduced during melt the ice compacts too easily, resulting in the correct area but too low extent. This issue is currently under investigation.

The spatial distribution of concentration is shown in Fig. 15. The concentration map shows that the sea ice distribution at minimum extent is well captured. The largest differences between the modelled and observed ice extent occur in the regions where the modelled ice concentration is low and the ice is easily influenced by the wind. Kauker et al. (2009) have shown the shape of the ice extent minimum to be heavily influenced by the wind, but we have not investigated this in our model.

In addition to concentration, Fig. 16 shows the spatial distribution of ice thickness at the beginning of the simulation, in mid-winter and at the sea ice minimum. These clearly show the high degree of heterogeneity that appears in the model, despite very smooth initial conditions. The mid-winter map shows substantial amounts of fracturing and ridge formation in the Beaufort Gyre and the Transpolar Drift Stream in particular. This heterogeneity persists until the end of the melt season, even if the melt does smooth it out somewhat.

neXtSIM: a new Lagrangian sea ice model

P. Rampal et al.

Title Page	
Abstract	Introduction
Conclusions	References
Tables	Figures
◀	▶
◀	▶
Back	Close
Full Screen / Esc	
Printer-friendly Version	
Interactive Discussion	



In order to evaluate the performance of neXtSIM we used a full Arctic setup and ran the model for 13 months, starting on 15 September 2008, and using realistic atmospheric forcing. The main evaluation results are:

- the model reproduces well the local motion of sea ice that is in “free-drift”;
- the model also reproduces well the drift of the pack ice, at local (~ 10 km) and large (Arctic-wide) spatial scales, and for daily to seasonal time scales;
- the model captures the observed spatial multifractal scaling of sea ice deformation over 3 orders of magnitude, from ~ 10 to ~ 1000 km, as well as its variability from winter to summer;
- the model captures the observed intermittency of sea ice deformation over two orders of magnitude, from 1 to ~ 100 days;
- the model produces seasonal cycles of sea ice volume, area, and extent that are all in good agreement with observations.

In conclusion, neXtSIM performs very well with respect to the most important metrics we can impose on sea ice model performance. Work still remains to improve the model, both in its representation of sea ice physics and in terms of numerical performance. We believe though that in its current stage of development neXtSIM has substantial potential as a general sea ice model. We therefore think that this new model could be a powerful tool for both the scientific and engineering communities. It can prove useful to develop and test new parameterisations of sea ice physical processes and to study the processes involved in the complex interactions between sea ice and the ocean, ecosystems, or the atmosphere. Ultimately neXtSIM may prove to be a powerful tool to be used to better understand the recent evolutions of Arctic and Antarctic sea ice covers as well as to predict their future.

Acknowledgements. We would like to acknowledge T. Williams and P. Griewank for interesting discussions and their contribution to the overall model development. This work was funded

neXtSIM: a new Lagrangian sea ice model

P. Rampal et al.

Title Page	
Abstract	Introduction
Conclusions	References
Tables	Figures
◀	▶
◀	▶
Back	Close
Full Screen / Esc	
Printer-friendly Version	
Interactive Discussion	



neXtSIM: a new Lagrangian sea ice model

P. Rampal et al.

Title Page

Abstract

Introduction

Conclusions

References

Tables

Figures



Back

Close

Full Screen / Esc

Printer-friendly Version

Interactive Discussion



- Comiso, J. C.: Bootstrap Sea Ice Concentrations from Nimbus-7 SMMR and DMSP SSM/I-SSMIS, Version 2, doi:10.5067/J6JQLS9EJ5HU, updated 2015, 2000. 5912
- Compère, G., Remacle, J. F., and Marchandise, E.: Transient Mesh Adaptivity with Large Rigid-Body Displacements, in: Proceedings of the 17th International Meshing Roundtable, edited by: Garimella, R., Springer, Berlin, 213–230, 2008. 5900
- Compère, G., Remacle, J.-F., Jansson, J., and Hoffman, J.: A mesh adaptation framework for dealing with large deforming meshes, *Int. J. Numer. Meth. Eng.*, 82, 843–867, doi:10.1002/nme.2788, 2009. 5900
- Connolley, W. M., Gregory, J. M., Hunke, E. C., and McLaren, A. J.: On the consistent scaling of terms in the sea-ice dynamics equation, *J. Phys. Oceanogr.*, 34, 1776–1780, 2004. 5893
- Coon, M. D., Maykut, G. A., Pritchard, R. S., Rothrock, D. A., and Thorndike, A. S.: Modeling the pack ice as an elastic plastic material, *AIDJEX Bull.*, 24, 1–105, 1974. 5888
- Dansereau, V., Weiss, J., Saramito, P., Lattes, P., and Coche, E.: A Maxwell elasto-brittle rheology for sea ice modeling, *Mercator Newsletter*, 35–40, 2015. 5889
- Dee, D. P., Uppala, S. M., Simmons, A. J., Berrisford, P., Poli, P., Kobayashi, S., Andrae, U., Balmaseda, M. A., Balsamo, G., Bauer, P., Bechtold, P., Beljaars, A. C. M., van de Berg, L., Bidlot, J., Bormann, N., Delsol, C., Dragani, R., Fuentes, M., Geer, A. J., Haimberger, L., Healy, S. B., Hersbach, H., Hólm, E. V., Isaksen, L., Kållberg, P., Köhler, M., Matricardi, M., McNally, A. P., Monge-Sanz, B. M., Morcrette, J. J., Park, B. K., Peubey, C., de Rosnay, P., Tavolato, C., Thépaut, J. N., and Vitart, F.: The ERA-Interim reanalysis: configuration and performance of the data assimilation system, *Q. J. Roy. Meteorol. Soc.*, 137, 553–597, 2011. 5905
- Ebert, E. E. and Curry, J. A.: An intermediate one-dimensional thermodynamic sea ice model for investigating ice–atmosphere interactions, *J. Geophys. Res.*, 98, 10085–10109, 1993. 5898
- EUMETSAT Ocean and Sea Ice Satellite Application Facility: Global sea ice concentration reprocessing dataset 1978–2015 (v1.2), available at: <http://osisaf.met.no>, last access: 1 June 2015. 5912
- Flocco, D. and Feltham, D. L.: A continuum model of melt pond evolution on Arctic sea ice, *J. Geophys. Res.*, 112, C08016, doi:10.1029/2006JC003836, 2007. 5888
- Gill, A. E.: *Atmosphere-Ocean Dynamics*, International Geophysics Series, Academic Press, London, 1982. 5898

neXtSIM: a new Lagrangian sea ice model

P. Rampal et al.

Title Page

Abstract

Introduction

Conclusions

References

Tables

Figures



Back

Close

Full Screen / Esc

Printer-friendly Version

Interactive Discussion



ocean modeling and geological, geophysical and oceanographic analyses, *Geophys. Res. Lett.*, 35, L07602, doi:10.1029/2008GL033520, 2008. 5902

Kagan, Y. Y.: Fractal dimension of brittle fracture, *J. Nonlinear Sci.*, 1, 1–16, 1991. 5890

Kagan, Y. Y. and Jackson, D. D.: Long-term earthquake clustering, *Geophys. J. Int.*, 104, 117–133, 1991. 5890

Kaleschke, L., Lüpkes, C., Vihma, T., Haarpaintner, J., Bochart, A., Hartmann, J., and Heygster, G.: SSM/I Sea Ice Remote Sensing for Mesoscale Ocean-Atmosphere Interaction Analysis, *Can. J. Remote Sens.*, 27, 526–537, 2001. 5912

Kauker, F., Kaminski, T., Karcher, M., Giering, R., Gerdes, R., and Voßbeck, M.: Adjoint analysis of the 2007 all time Arctic sea-ice minimum, *Geophys. Res. Lett.*, 36, L03707, doi:10.1029/2008GL036323, 103707, 2009. 5913

Kwok, R., Curlander, J. C., McConnell, R., and Pang, S. S.: An Ice Motion Tracking System at the Alaska SAR Facility, *IEEE J. Ocean. Eng.*, 15, 44–54, 1990. 5903

Kwok, R., Cunningham, G. F., and Pang, S. S.: Fram Strait sea ice outflow, *J. Geophys. Res.*, 109, C01009, doi:10.1029/2003JC001785 2004. 5911

Larour, E., Seroussi, H., Morlighem, M., and Rignot, E.: Continental scale, high order, high spatial resolution, ice sheet modelling using the Ice Sheet System Model (ISSM), *J. Geophys. Res.-Earth*, 117, F01022, doi:10.1029/2011JF002140, 2012. 5901

Lemieux, J. F., Tremblay, B., Sedlacek, J., Tupper, P., Thomas, S., D, H., and Auclair, J. P.: Improving the numerical convergence of viscous-plastic sea ice models with the Jacobian-free Newton-Krylov method, *J. Comp. Phys.*, 229, 2840–2852, 2010. 5889

Lemieux, J.-F., Tremblay, B. L., Dupont, F., Plante, M., Smith, G. C., and Dumont, D.: A basal stress parameterization for modeling landfast ice, *J. Geophys. Res.-Oceans*, 120, 3157–3173, 2015. 5895

Lindsay, R. and Schweiger, A.: Arctic sea ice thickness loss determined using subsurface, aircraft, and satellite observations, *The Cryosphere*, 9, 269–283, doi:10.5194/tc-9-269-2015, 2015. 5886

Lipscomb, W. H., Hunke, E. C., Maslowski, W., and Jakacki, J.: Ridging, strength, and stability in high-resolution sea ice models, *J. Geophys. Res.*, 112, C03S91, doi:10.1029/2005JC003355, 2007. 5888

Lu, P., Leppäranta, M., Li, Z., and Cheng, B.: A parameterization of the ice-ocean drag coefficient, *J. Geophys. Res.*, 116, C07019, doi:10.1029/2010JC006878, 2011. 5889

neXtSIM: a new Lagrangian sea ice model

P. Rampal et al.

Title Page

Abstract

Introduction

Conclusions

References

Tables

Figures

◀

▶

◀

▶

Back

Close

Full Screen / Esc

Printer-friendly Version

Interactive Discussion



- Lüpkes, C., Gryanik, V. M., Hartmann, J., and Andreas, E. L.: A parametrization, based on sea ice morphology, of the neutral atmospheric drag coefficients for weather prediction and climate models, *J. Geophys. Res.-Atmos.*, 117, D13112, doi:10.1029/2012JD017630, 2012. 5889
- 5 Marsan, D. and Weiss, J.: Space/time coupling in brittle deformation at geophysical scales, *Earth Planet. Sc. Lett.*, 296, 353–359, 2010. 5890
- Marsan, D., Stern, H. L., Lindsay, R., and Weiss, J.: Scale dependence and localization of the deformation of Arctic sea ice, *Phys. Rev. Lett.*, 93, 178501, 2004. 5890, 5908, 5909
- Maykut, G. A. and Untersteiner, N.: Some results form time-dependent thermodynamic model
10 of sea ice, *J. Geophys. Res.*, 76, 1550–1575, 1971. 5887, 5898
- McPhee, M. G.: The Effect of the Oceanic Boundary Layer on the Mean Drift of Pack Ice: Application of a Simple Model, *J. Phys. Oceanogr.*, 9, 388–400, 1979. 5905
- Ólason, E. and Notz, D.: Drivers of variability in Arctic sea-ice drift speed, *J. Geophys. Res.-Oceans*, 119, 5755–5775, doi:10.1002/2014JC009897, 2014. 5907
- 15 Polar Group: Polar Atmosphere-Ice-Ocean Processes – a Review of Polar Problems in Climate Research, *Rev. Geophys. Space GE.*, 18, 525–543, 1980. 5887
- Rabatel, M., Labbé, S., and Weiss, J.: Dynamics of an Assembly of Rigid Ice Floes, *J. Geophys. Res.-Oceans*, 120, 5887–5909, doi:10.1002/2015JC010909, 2015. 5889
- Rampal, P., Weiss, J., Marsan, D., Lindsay, R., and Stern, H. L.: Scaling properties of
20 sea ice deformation from buoy dispersion analysis, *J. Geophys. Res.*, 113, C03002, doi:10.1029/2007JC004143, 2008. 5890, 5908, 5909, 5910
- Rampal, P., Weiss, J., and Marsan, D.: Positive trend in the mean speed and deformation rate of Arctic sea ice, 1979–2007, *J. Geophys. Res.*, 114, C05013, doi:10.1029/2008JC005066, 2009. 5887, 5907
- 25 Rampal, P., Weiss, J., Dubois, C., and Campin, J. M.: IPCC climate models do not capture Arctic sea ice drift acceleration: Consequences in terms of projected sea ice thinning and decline, *J. Geophys. Res.*, 116, C00D07, doi:10.1029/2011JC007110, 2011. 5887
- Richardson, L. F. and Stommel, H.: Note on eddy diffusion in the sea, *J. Meteorol.*, 5, 238–240, 1948. 5909
- 30 Rothrock, D. A.: The energetics of the plastic deformation of pack ice by ridging, *J. Geophys. Res.*, 80, 1975. 5888

neXtSIM: a new Lagrangian sea ice model

P. Rampal et al.

Title Page

Abstract

Introduction

Conclusions

References

Tables

Figures



Back

Close

Full Screen / Esc

Printer-friendly Version

Interactive Discussion



- Sakov, P., Counillon, F., Bertino, L., Lisæter, K. A., Oke, P. R., and Korablev, A.: TOPAZ4: an ocean-sea ice data assimilation system for the North Atlantic and Arctic, *Ocean Sci.*, 8, 633–656, doi:10.5194/os-8-633-2012, 2012. 5901
- Sakov, P., Counillon, F., Bertino, L., Finck, N., and Renkl, C.: Quality Information Document For Arctic Physical Reanalysis Product – EU Copernicus Marine Service, Tech. rep., Bergen, 2015. 5903
- Schreyer, H. L., Sulsky, D., Munday, L. B., Coon, M., and Kwok, R.: Elastic-decohesive constitutive model for sea ice, *J. Geophys. Res.*, 111, C11S26, doi:10.1029/2005JC003334, 2006. 5889
- Schulson, E. M.: Fracture of Ice and other Coulombic Materials, *Mechanics of Natural Solids*, Springer, Berlin, Heidelberg, p. 177, 2009.
- Schweiger, A., Lindsay, R., Zhang, J., Steele, M., Stern, H., and Kwok, R.: Uncertainty in modeled Arctic sea ice volume, *J. Geophys. Res.-Oceans*, 116, C00D06, doi:10.1029/2011JC007084, c00D06, 2011. 5911
- Semtner, A. J.: A model for the thermodynamic growth of sea ice in numerical investigations of climate, *J. Phys. Oceanogr.*, 6, 379–389, 1976. 5887, 5898
- Sirevaag, A., de la Rosa, S., Fer, I., Nicolaus, M., Tjernström, M., and McPhee, M. G.: Mixing, heat fluxes and heat content evolution of the Arctic Ocean mixed layer, *Ocean Sci.*, 7, 335–349, doi:10.5194/os-7-335-2011, 2011. 5902
- Spreen, G., Kaleschke, L., and Heygster, G.: Sea ice remote sensing using AMSR-E 89-GHz channels, *J. Geophys. Res.-Oceans*, 113, C02S03, doi:10.1029/2005JC003384, 2008. 5912
- Stern, H. L. and Lindsay, R.: Spatial scaling of Arctic sea ice deformation, *J. Geophys. Res.*, 114, C10017, doi:10.1029/2009JC005380, 2009. 5910
- Stroeve, J., Barrett, A., Serreze, M., and Schweiger, A.: Using records from submarine, aircraft and satellites to evaluate climate model simulations of Arctic sea ice thickness, *The Cryosphere*, 8, 1839–1854, doi:10.5194/tc-8-1839-2014, 2014. 5887
- Sulsky, D., Schreyer, H., Peterson, K., Kwok, R., and Coon, M.: Using the material-point method to model sea ice dynamics, *J. Geophys. Res.*, 112, C02S90, doi:10.1029/2005JC003329, 2007. 5889
- Thorndike, A. S., Thorrock, D. A., Maykut, G. A., and Colony, R.: The thickness distribution of sea ice, *J. Geophys. Res.*, 80, 4501–4513, 1975. 5888, 5895
- Tremblay, L. B. and Mysak, L. A.: Modeling sea ice as a granular material, including the dilatancy effect, *J. Phys. Oceanogr.*, 27, 2342–2360, 1997. 5889

neXtSIM: a new Lagrangian sea ice model

P. Rampal et al.

Title Page

Abstract

Introduction

Conclusions

References

Tables

Figures



Back

Close

Full Screen / Esc

Printer-friendly Version

Interactive Discussion



Tsamados, M., Feltham, D. L., and Wilchinsky, A. V.: Impact of a new anisotropic rheology on simulations of Arctic sea ice, *J. Geophys. Res.*, 118, 91–107, doi:10.1029/2012JC007990, 2013. 5889

5 Tsamados, M., Feltham, D. L., Schroeder, D., Flocco, D., Farrell, S. L., Kurtz, N., Laxon, S. W., and Bacon, S.: Impact of Variable Atmospheric and Oceanic Form Drag on Simulations of Arctic Sea Ice, *J. Phys. Oceanogr.*, 44, 1329–1353, doi:10.1175/JPO-D-13-0215.1, 2014. 5889

Ukita, J. and Martinson, D. G.: An efficient adjustable-layering thermodynamic sea-ice model formulation for high-frequency forcing, *Ann. Glaciol.*, 33, 253–260, 2001. 5888

10 Vaughan, D., Comiso, J., Allison, I., Carrasco, J., Kaser, G., Kwok, R., Mote, P., Murray, T., Paul, F., Ren, J., Rignot, E., Solomina, O., Steffen, K., and Zhang, T.: Observations: Cryosphere, book section 4, Cambridge University Press, Cambridge, United Kingdom and New York, NY, USA, doi:10.1017/CBO9781107415324.012, 317–382, 2013. 5887

15 Wang, L. R. and Ikeda, M.: A Lagrangian description of sea ice dynamics using the finite element method, *Ocean Model.*, 7, 21–38, 2004. 5899

Warren, S. G., Rigor, I. G., Untersteiner, N., Radionov, V. F., Bryazgin, N. N., Aleksandrov, Y. I., and Colony, R.: Snow Depth on Arctic Sea Ice, *J. Climate*, 12, 1814–1829, doi:10.1175/1520-0442(1999)012<1814:SDOASI>2.0.CO;2, 1999. 5903

20 Weiss, J. and Schulson, E. M.: Coulombic faulting from the grain scale to the geophysical scale: Lessons from ice, *J. Phys. D Appl. Phys.*, 42, 214017, 2009. 5894

Weiss, J., Stern, H. L., and Schulson, E. M.: Sea ice rheology from in-situ, satellite and laboratory observations: Fracture and friction, *Earth Planet. Sc. Lett.*, 255, 1–8, 2007. 5894

25 Weiss, J., Marsan, D., and Rampal, P.: Space and time scaling laws induced by the multiscale fracturing of the Arctic sea ice cover, in: IUTAM Symposium on Scaling Laws in Ice Mechanics and Ice Dynamics, Springer Netherlands, 101–109, 2009. 5889

Wilchinsky, A. V. and Feltham, D.: Modelling the rheology of sea ice as a collection of diamond-shaped oes, *J. Non-Newton Fluid*, 138, 22–32, 2006. 5889

Winton, M.: A reformulated three-layer sea ice model, *J. Atmos. Ocean. Tech.*, 17, 525–531, 2000. 5888

30 Zhang, J. and Rothrock, D.: Modeling global sea ice with a thickness and enthalpy distribution model in generalized curvilinear coordinates, *Mon. Weather Rev.*, 131, 845–861, 2003. 5903

neXtSIM: a new Lagrangian sea ice model

P. Rampal et al.

Title Page

Abstract

Introduction

Conclusions

References

Tables

Figures

◀

▶

◀

▶

Back

Close

Full Screen / Esc

Printer-friendly Version

Interactive Discussion



Table 1. List of variables used in neXtSIM.

Symbol	Name	Meaning	Unit
h	sea ice thickness	volume of ice per unit area	m
h_s	snow thickness	volume of snow per unit area	m
A	sea ice concentration	surface of ice per unit area	–
d	sea ice damage	0 = undamaged, 1 = completely damaged ice	–
u	sea ice velocity	horizontal sea ice velocity	ms^{-1}
σ	sea ice internal stress	planar internal stress	Nm^{-2}

**neXtSIM: a new
Lagrangian sea ice
model**

P. Rampal et al.

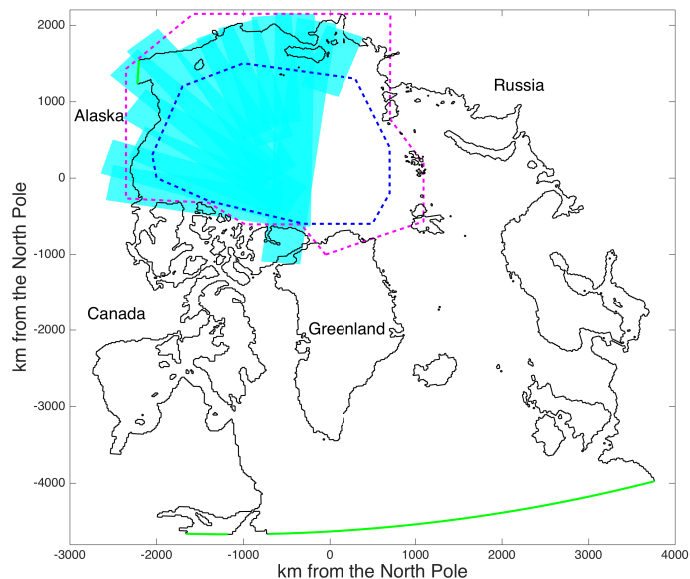


Figure 1. Model domain projected on a polar stereographic plane with open boundaries in green. The region delimited by the dashed blue line and the cyan area are used to compute the drift and deformation statistics. The dashed line in magenta shows the area for which the mean ice thickness and ice volume time series are calculated.

Title Page

Abstract

Introduction

Conclusions

References

Tables

Figures



Back

Close

Full Screen / Esc

Printer-friendly Version

Interactive Discussion



neXtSIM: a new Lagrangian sea ice model

P. Rampal et al.

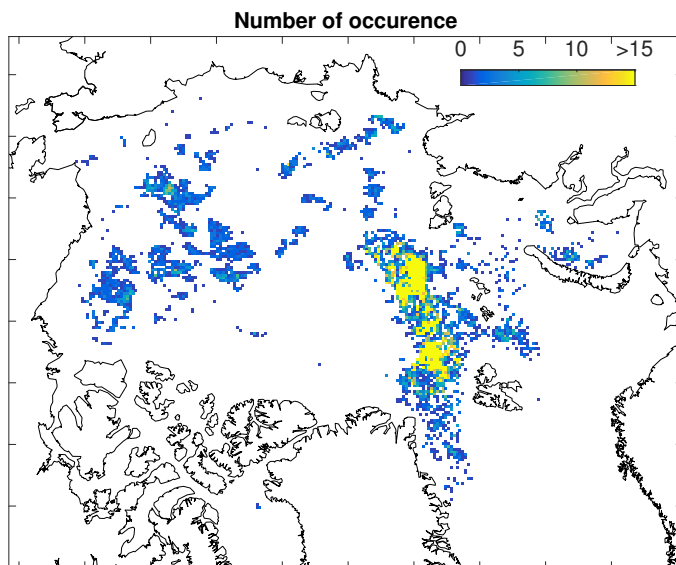


Figure 2. Number of occurrence of free drift events identified between 31 October 2007 and 28 April 2008 and selected for the optimisation of the air drag parameter.

[Title Page](#)[Abstract](#)[Introduction](#)[Conclusions](#)[References](#)[Tables](#)[Figures](#)[Back](#)[Close](#)[Full Screen / Esc](#)[Printer-friendly Version](#)[Interactive Discussion](#)

**neXtSIM: a new
Lagrangian sea ice
model**

P. Rampal et al.

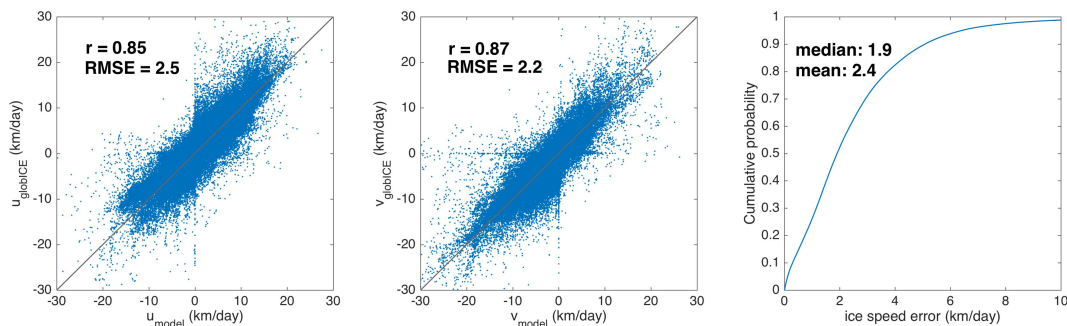


Figure 4. Scatter plots for the two components of all the simulated and observed drift vectors between 31 October 2007 and 28 April 2008 (left and middle panels). Cumulative distribution of all the velocity errors (right panel).

[Title Page](#)[Abstract](#)[Introduction](#)[Conclusions](#)[References](#)[Tables](#)[Figures](#)[Back](#)[Close](#)[Full Screen / Esc](#)[Printer-friendly Version](#)[Interactive Discussion](#)

neXtSIM: a new Lagrangian sea ice model

P. Rampal et al.

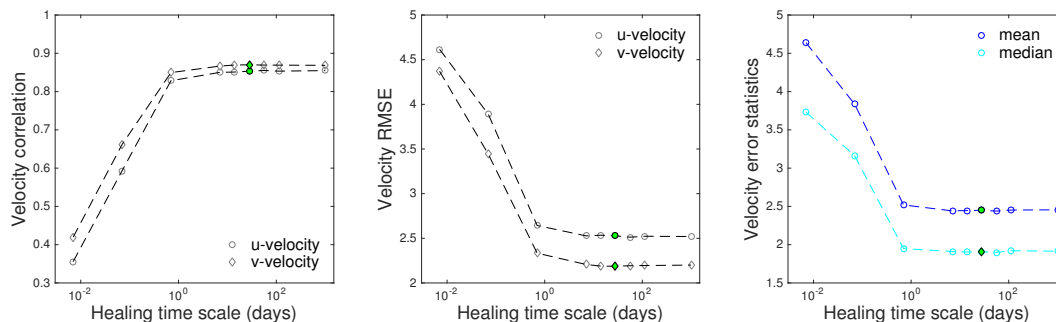


Figure 5. Sensitivity of the velocity statistics to the healing time scale. The left panel shows the correlation between the simulated and observed ice drift, the central panel shows the RMSE and the right panel the velocity mean and median velocity errors. The dots in green correspond to the reference run (28 days healing time scale).

**neXtSIM: a new
Lagrangian sea ice
model**

P. Rampal et al.

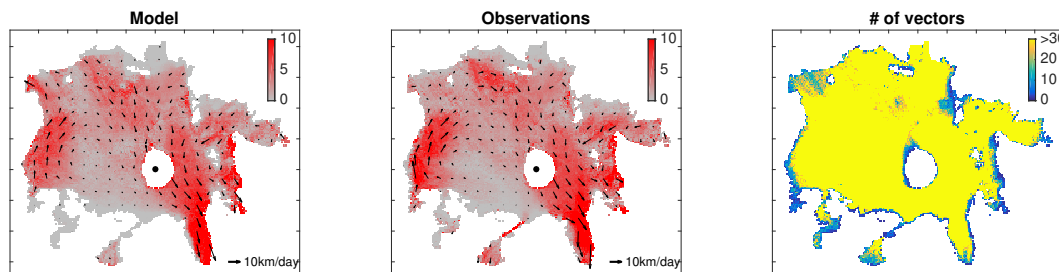


Figure 6. Simulated and observed ice drift averaged over the period between 31 October 2007 and 28 April 2008 (left and middle panels). The number of observations is shown in the right panel. The mean fields are build on a regular grid having a resolution of 21 km and are computed by averaging the components of the simulated and observed drift vectors used for the scatter plot. Note that the color scale for the number of observations is capped at 30 to show that some regions are poorly covered by data.

[Title Page](#)[Abstract](#)[Introduction](#)[Conclusions](#)[References](#)[Tables](#)[Figures](#)[◀](#)[▶](#)[◀](#)[▶](#)[Back](#)[Close](#)[Full Screen / Esc](#)[Printer-friendly Version](#)[Interactive Discussion](#)

**neXtSIM: a new
Lagrangian sea ice
model**

P. Rampal et al.

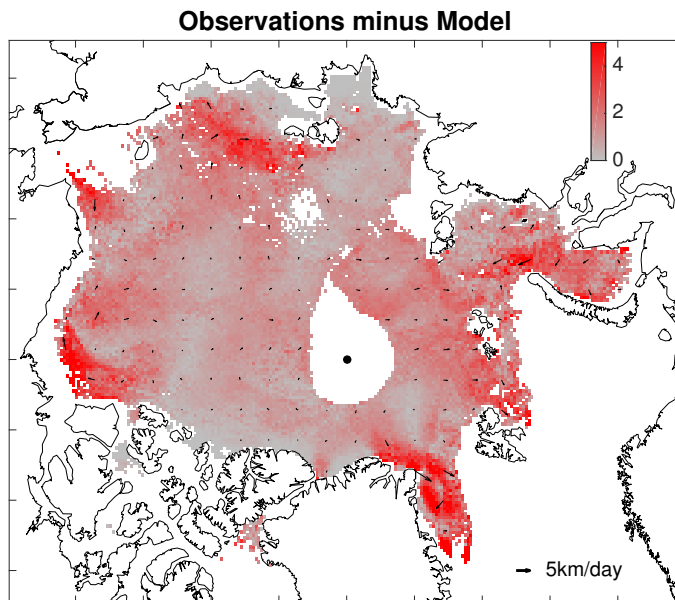


Figure 7. Difference between the observed and simulated mean ice drift shown on Fig. 6. The cells with less than 30 observations over the winter are masked. Systematic errors are located in the Beaufort Gyre and Fram Strait and in some areas of the Kara, East Siberian and Chukchi Seas. In the rest of the domain the error on the mean winter drift is only about 1 km day^{-1} .

[Title Page](#)[Abstract](#)[Introduction](#)[Conclusions](#)[References](#)[Tables](#)[Figures](#)[◀](#)[▶](#)[◀](#)[▶](#)[Back](#)[Close](#)[Full Screen / Esc](#)[Printer-friendly Version](#)[Interactive Discussion](#)

neXtSIM: a new Lagrangian sea ice model

P. Rampal et al.

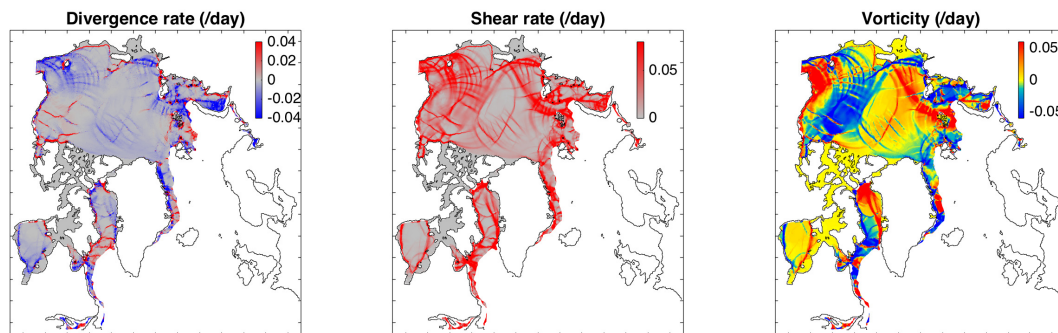


Figure 9. Example of deformation fields simulated by neXtSIM. The divergence rate, shear rate and vorticity are computed from the Lagrangian displacement simulated between 20 and 21 February 2008. One could note that large divergence rate coincide with large shear rate and that landfast ice is present on the Siberian coast and east of Kara Sea.

[Title Page](#)[Abstract](#)[Introduction](#)[Conclusions](#)[References](#)[Tables](#)[Figures](#)[Back](#)[Close](#)[Full Screen / Esc](#)[Printer-friendly Version](#)[Interactive Discussion](#)

neXtSIM: a new Lagrangian sea ice model

P. Rampal et al.

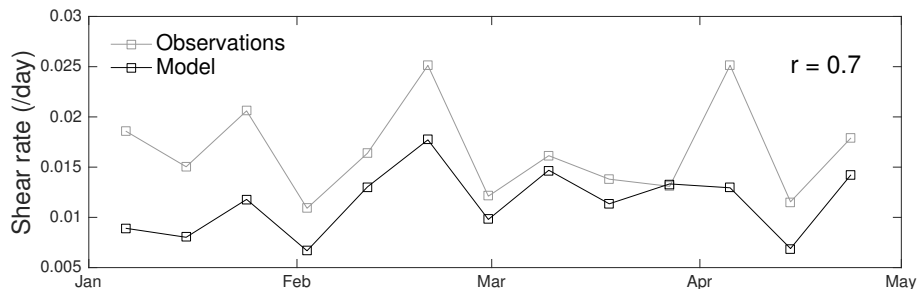


Figure 10. Mean value of the shear rate distributions corresponding to 13 periods of 9 days between January and May 2008. The deformation rates are computed at a spatial scale of 20 km for matching times and locations between the observation and the model following the same procedure as in Bouillon and Rampal (2015a).

[Title Page](#)
[Abstract](#)
[Introduction](#)
[Conclusions](#)
[References](#)
[Tables](#)
[Figures](#)

[Back](#)
[Close](#)
[Full Screen / Esc](#)
[Printer-friendly Version](#)
[Interactive Discussion](#)


neXtSIM: a new Lagrangian sea ice model

P. Rampal et al.

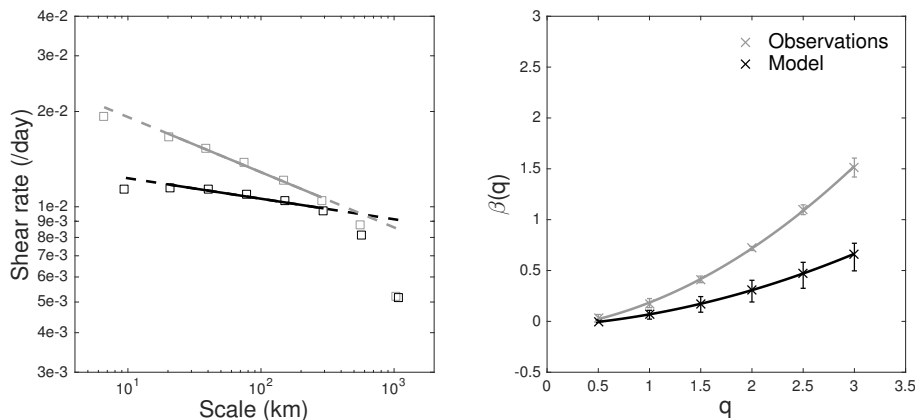


Figure 11. Scaling analysis of sea ice deformation performed for the period January–May. The left panel shows the mean shear rate computed for spatial scales ranging from ~ 10 to 1000 km. A power law $\langle \dot{\epsilon} \rangle \sim L^{-\beta}$ is fitted to the data sets (grey and black lines). The departure from the power law fit at $L < 20$ km and $L > 500$ km comes from finite size effect (model/data resolutions and size of the Arctic basin, respectively). The scaling exponents $\beta(q)$ for the other moment orders of the shear distribution are shown in the right panel. These values fit remarkably well with a quadratic function, which reveals the multi-fractal character of the scaling. The error bars correspond to the minimum and maximum exponents computed over two consecutive scales.

neXtSIM: a new Lagrangian sea ice model

P. Rampal et al.

Title Page

Abstract

Introduction

Conclusions

References

Tables

Figures



Back

Close

Full Screen / Esc

Printer-friendly Version

Interactive Discussion

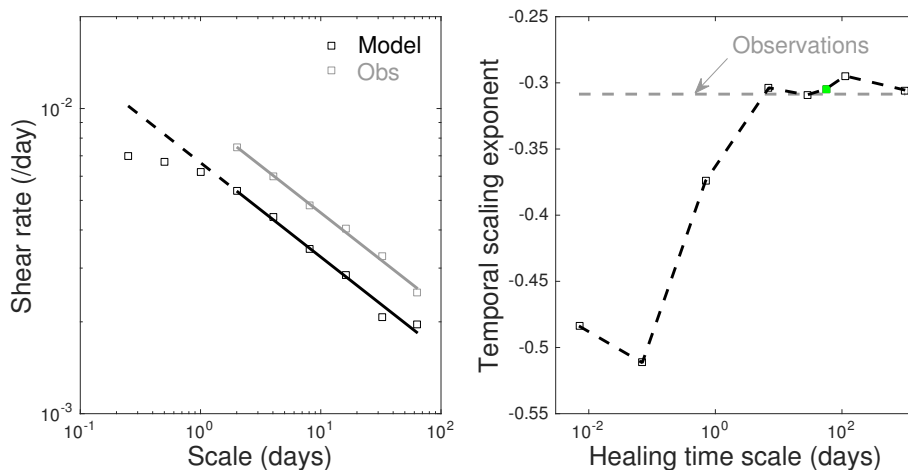


Figure 12. Temporal scaling analysis of sea ice deformation performed for the period January–May. Left panel shows a proxy of deformation rate (defined as in Rampal et al., 2008) computed for temporal scales ranging from 6 h to 60 days. A power law fit $\langle \dot{\epsilon} \rangle \sim T^{-\alpha}$ is calculated for the data sets (grey and black lines) and the scaling exponent is found being very similar between the model and the observations. This shows the model captures the observed intermittency of sea ice deformation. Right panel shows the sensitivity of the scaling exponent to the healing time scale. The green square corresponds to the exponent obtained for the reference run (shown on left panel).

neXtSIM: a new Lagrangian sea ice model

P. Rampal et al.

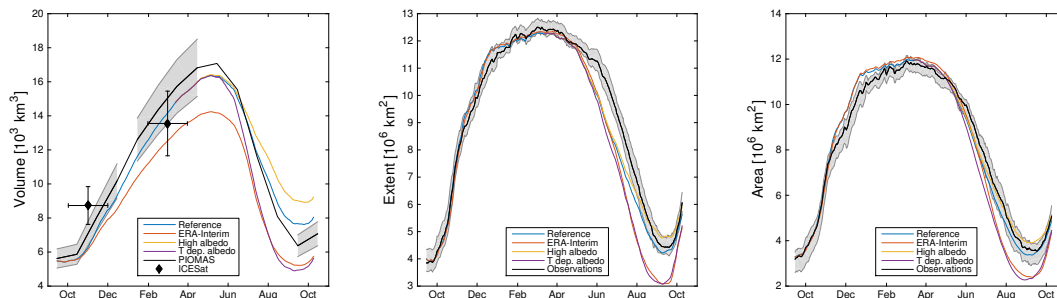


Figure 14. Modelled seasonal cycle in volume (left panel), extent (centre panel), and area (right panel). The volume is calculated within the area covered by the ICESat observations (1) and can be compared to the ICESat and PIOMAS results. The extent and area are calculated within the model grid and can be compared to the AMSR-E observations (for further details see text).

[Title Page](#)
[Abstract](#)
[Introduction](#)
[Conclusions](#)
[References](#)
[Tables](#)
[Figures](#)

[Back](#)
[Close](#)
[Full Screen / Esc](#)
[Printer-friendly Version](#)
[Interactive Discussion](#)

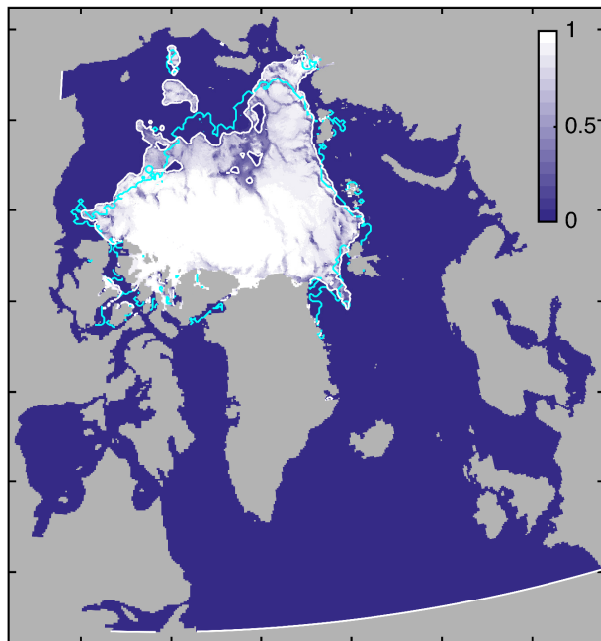



Figure 15. Modelled ice concentration at the observed extent minimum (19 September 2008). Overlaid are lines for the modelled and observed (AMSR-E) 15% concentration limit in white and cyan, respectively.

neXtSIM: a new
Lagrangian sea ice
model

P. Rampal et al.

Title Page

Abstract

Introduction

Conclusions

References

Tables

Figures



Back

Close

Full Screen / Esc

Printer-friendly Version

Interactive Discussion



**neXtSIM: a new
Lagrangian sea ice
model**

P. Rampal et al.

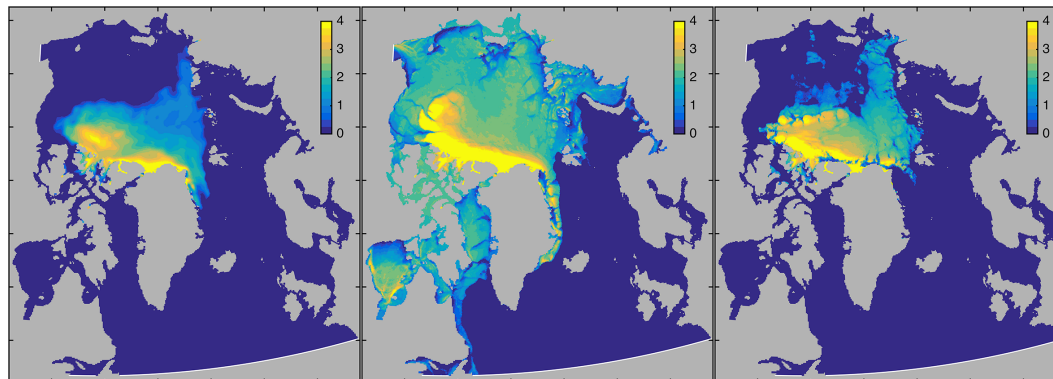


Figure 16. Ice thickness per unit area for the initial conditions (left panel), the model state at mid-winter (centre panel), and the model state at observed extent minimum (right panel). Note the increasing heterogeneity in the sea ice thickness field emerging from the new physics included in the model.

[Title Page](#)[Abstract](#)[Introduction](#)[Conclusions](#)[References](#)[Tables](#)[Figures](#)[◀](#)[▶](#)[◀](#)[▶](#)[Back](#)[Close](#)[Full Screen / Esc](#)[Printer-friendly Version](#)[Interactive Discussion](#)